Fundamental Aspects of Semiconductor Device Modeling Associated with Discrete Impurities: Drift-Diffusion Simulation Scheme

Nobuyuki Sano, *Member, IEEE, Katsuhisa Yoshida, Kohei Tsukahara, and Gyutae Park*

***Abstract*— We discuss the fundamental aspects of how discrete impurities could be physically modeled under the framework of the Drift-Diffusion (DD) simulations. The detailed physical interpretations of potential fluctuations, impurity-limited mobility, and an appropriate modeling to represent the discrete nature of impurities are explained. The present analyses are validated by DD simulations with various types of discrete impurity models. The traditional mobility model which reproduces the experimental mobility at various impurity densities could be used in our long-range discrete impurity model, whereas localized impurity models in which impurity charge is spatially localized at each impurity site induce unphysical polarization fields in semiconductor substrate and are unable to predict the correct mobility.**

***Index Terms*— random dopant fluctuation (RDF), discrete impurity, hydrodynamic limit, Drift-Diffusion simulation, Coulomb interaction**

I. Introduction

The pursuit of scaling merit of silicon-based electron devices is being under progress in nano-meter regimes and, as a result, the role of device simulation gets more and more important to predict reliable device characteristics [1]. Among the issues related to device simulations, reliable predictions of random dopant fluctuations (RDFs) are of critical importance because they are a dominant factor that prevents further miniaturization of silicon-based electron devices [2]. In the past few decades, intensive simulation studies on RDFs have been carried out by the DD simulation scheme [3]–[10]. However, an introduction of discrete impurities into DD simulations has some ambiguity: Since the RDFs result from the discrete nature of impurities, it is critically dependent on how discrete impurities are represented in the DD simulations. We have recently revisited this problem to clarify the physics behind RDFs in the DD simulation scheme [11], [12].

A key to understand the physics of RDFs lies in the fact that ionized impurities are not completely screened by free carriers during device operation and it is an unscreened part of the impurity potential that shows up as potential fluctuations responsible to the variabilities in device characteristics [12]. Hence, the potential fluctuations could be identified as the "long-range" part of the impurity potential whose wavelength is greater than the screening length. On the other hand, the short-range part of the impurity potential should be explicitly excluded from the Poisson equation to avoid the double-count in both the Poisson and current-continuity equations.

However, there is still ambiguity in the usage of a traditional mobility model under discrete impurities [11], in which the electron mobility is parametrized as a function of impurity density to reproduce the experimental mobility in bulk. For example, the concept of mobility clearly breaks down near threshold at very low temperature where the current is dominated by percolation paths. In decano-scale devices, the mean-free-path of carriers is comparable to or even larger than the characteristic length over which potential and density change so that local equilibrium, and hence hydrodynamic approximation, breaks down. Although the concept of mobility inherently has a limitation to describe the correct transport characteristics, the device properties are dominated by electrostatics.

Nevertheless, the usage of improper mobility in DD simulations leads to unphysical device characteristics, as we shall demonstrate in the present paper. This results from the fact that the impurity density used to extract the value of mobility from the mobility model is not clear because impurity density is either spatially localized or artificially spread in the substrate, depending on the discrete impurity model employed in the simulations [13]. In the present paper, we address this issue and show that the mobility could be directly evaluated with the impurity density in our discrete impurity model. Our claims are then justified by performing the DD simulations under various types of impurity models.

II. Discrete Impurity in Drift-Diffusion Simulation

A. Interpretation of Potential Fluctuations

Firstly, we would like to stress that the equations in the DD simulations are derived from the Boltzmann transport equation under local equilibrium approximation (hydrodynamic limit) [14], [15] and, thus, the physical quantities such as potential, density, and current density are expressed as continuous and smooth functions of position. This is equivalent to saying that the spatial resolution is limited by a mean-free-path of dominant scattering in the substrate [6], [7].

To represent the discrete nature of impurity, we assume, for simplicity, that each impurity is represented by a point charge.

This work was supported in part by KIOXIA Corporation (former Toshiba Memory Corporation).

The authors are with the Institute of Applied Physics, University of Tsukuba, Tsukuba, Ibaraki 305-8573 Japan (e-mail: sano.nobuyuki.gw@u.tsukuba.ac.jp).

Then, the "microscopic" impurity density is expanded by the Fourier series as

$$N_{imp}^{micro}(\mathbf{r}) = \frac{m}{\Delta V} + \sum_{i=1}^{m} \frac{1}{\Delta V} \sum_{\mathbf{k}\neq 0} e^{i\mathbf{k}\cdot(\mathbf{r}-\mathbf{R}_i)}, \qquad (1)$$

where m is the number of impurities included in a small volume ΔV around the position $\mathbf{r}$, and $\mathbf{R}_i$ is the position vector of the i-th impurity. The first term is the impurity density corresponding to the zero-Fourier component and the second represents the density fluctuations due to the discrete nature of impurities. Notice that the macroscopic impurity density $\bar{N}_{imp}$, denoted as the "jellium" impurity density hereafter, is given by averaging $N_{imp}^{micro}(\mathbf{r})$ over all possible impurity configurations in ΔV. Hence, $\bar{N}_{imp}$ $(= m/\Delta V)$ becomes identical to the zero-Fourier component of $N_{imp}^{micro}(\mathbf{r})$. This implies that all non-zero Fourier components of the impurity potential are regarded as scattering potential in the traditional DD simulations and taken into account through the mobility model implemented in the current-continuity equation. However, the impurity-limited mobility is, in most cases, evaluated by Yukawa's screened Coulomb potential and only the Fourier components whose wavelength is smaller than the screening length are treated as scattering potential. The rest of the non-zero Fourier components, denoted as the long-range part of the impurity potential, is assumed to be screened by carriers and, thus, completely ignored in DD simulations.

The above scenario, however, holds true only if the equilibrium condition along with the overall charge neutrality is fulfilled. Near threshold voltages in MOSFETs, the channel region is depleted and the assumption of "complete screening" breaks down, and, hence, the long-range part of the impurity potential shows up as potential fluctuations. To represent the discrete nature of impurities, we need to introduce this unmasked part of the impurity potential *explicitly* into the Poisson equation. The short-range part of the impurity potential must be excluded from the Poisson equation to avoid the double-count in both the Poisson and current-continuity equations, although other length scales such as mean-free-path and mean separation of impurities are also involved in taking account of the details of scattering process.

B. Discrete Impurity Model for Drift-Diffusion Simulations

We notice that the long-range part of the impurity potential is identical (except its charge polarity) to the potential induced by excess carriers around impurities for screening. Therefore, if each impurity charge is spread in space and represented in accordance with the induced carrier density in the Poisson equation, the impurity charge density exactly cancels with that of induced carriers and the resulting electrostatic potential under equilibrium reduces to that of the jellium impurity. In the subthreshold regimes, on the other hand, an unscreened part of the impurity potential shows up as potential fluctuations. The impurity density is then derived by employing the linear approximation for screening and calculated by

$$\rho^{long}(\mathbf{q}) = -\varepsilon_s \mathbf{q}^2 \left(\frac{1}{\varepsilon(\mathbf{q})} - 1 \right) \phi_{bare}(\mathbf{q}), \qquad (2)$$

where ε_s is the static dielectric constant of the semiconductor substrate, $\phi_{bare}(\mathbf{q})$ is the bare Coulomb potential of an impurity, and $\varepsilon(\mathbf{q})$ is the (relative) dielectric function. The inverse Fourier transform of Eq. (2) is the impurity density in real space and referred to the (long-range) discrete impurity model. The details are presented in Ref. [12].

As a simple example, the discrete impurity model in bulk where boundary and interface of the semiconductor substrate are ignored is easily derived [11]. The result is given by

$$\rho^{long}(\mathbf{r}) = e\frac{{q_c}^2}{4\pi}\frac{e^{-q_c r}}{r}, \qquad (3)$$

where q_c is the inverse of the screening length. This is the discrete impurity density applicable to bulk structures. The electrostatic potential induced by Eq. (3) becomes the difference between the bare impurity potential and the Yukawa (scattering) potential. This is exactly what we have intended for the discrete impurity model consistent with the framework of the DD simulation. Notice that the electrostatic potential is "numerically" evaluated through DD simulations once each localized impurity is represented by the discrete impurity model such as Eq. (3) in the Poisson equation.

The present approach could be applied to more complicated structures where discrete impurities reside in nano-scale device structures so that the substrate is surrounded by boundary and/or interface. For such cases, the long-range part of the impurity potential is obtained by the charge density of the screening carriers (with opposite sign) under the influence of boundary and/or interface. The bare Coulomb potential of an impurity near interface is calculated by Green's function with appropriate boundary conditions and, thus, the discrete impurity density consistent with the device geometry is easily obtained from Eq. (2). The discrete impurity density near the gate-oxide interface has been studied along this line in Refs. [12], [16].

C. Interpretation of Mobility under Discrete Impurities

Since the impurity density artificially spreads in space in the discrete impurity model, it is not clear which impurity density should be referred to in evaluating mobility from the mobility model implemented in the current-continuity equation. To clarify this point, we first recall that the electrostatic potential appeared in the current-continuity equation corresponds to the long-range part of the impurity potential. Therefore, the drift velocity is driven by this long-range potential modulations. This is physically reasonable because drift velocity is an "average" velocity of electrons, in contrast with thermal velocity of individual electrons, and the long-range part of the Coulomb potential is indeed responsible to induce such collective behaviors of electrons. In other words, a clear distinction between the drift and thermal velocities is critical and to exclude the short-range part of the impurity potential from the Poisson equation is inevitable.

Another point is that the scattering time τ_n included in electron mobility, $\mu_n = e\tau_n/m$, is also an "average" quantity. In the regime of high impurity densities ($\geq 10^{18}$ cm^{-3}) with which we are mainly concerned in nanoscale devices, the Coulomb interaction, namely, impurity scattering and

TABLE I
IMPURITY'S MEAN-SEPARATION, SCREENING LENGTH AND LONG-RANGE POTENTIAL FLUCTUATIONS

N_{imp} (cm^{-3})	r_{ms} (nm)	λ_c (nm)	$e\Delta\phi$ (meV)
10^{17}	13.4	12.9	9.45
10^{18}	6.20	3.89	31.4
10^{19}	2.88	1.30	93.9
10^{20}	1.34	1.02	120

electron-electron scattering, dominates [17], [18]. Then, τ_n is averaged over the electron distribution function (weighted with energy) and over all possible configurations of impurities. The latter average results from an implicit assumption in impurity scattering that impurities are randomly distributed in the substrate. Therefore, the inverse of τ_n obtained from Fermi's golden rule is averaged over impurity configurations and the squared amplitude of the transition matrix becomes simply proportional to the "jellium" impurity density $\bar{N}_{imp}$;

$$\left\langle \left|V\left(\mathbf{q}\right)\right|^2 \right\rangle = \int_{\Delta V} \frac{d^3\mathbf{R}_1}{\Delta V} \cdots \frac{d^3\mathbf{R}_m}{\Delta V} \left| \frac{1}{\Delta V} \int d^3\mathbf{r}\, e^{-i\mathbf{q}\cdot\mathbf{r}} \sum_{i=1}^{m} \left(-e\right) \phi^{short}\left(\mathbf{r}-\mathbf{R}_i\right) \right|^2 = \frac{\bar{N}_{imp}}{\Delta V} \left| e\phi^{short}\left(\mathbf{q}\right) \right|^2, \tag{4}$$

where $\phi^{short}\left(\mathbf{r}-\mathbf{R}_i\right)$ is the short-range (scattering) potential due to the i-th impurity at $\mathbf{R}_i$ and $\phi^{short}\left(\mathbf{q}\right)$ is its Fourier transform. Hence, an explicit information of impurity position is lost (under the Born approximation) and the exact location of impurities in τ_n (and, thus, in μ_n) becomes irrelevant under the framework of the DD simulation. This implies that τ_n (or μ_n) is meaningful over the volume comparable to the mean-free-path of impurity scattering, which is roughly equal to impurity's mean-separation [19]. Since impurity's mean-separation is comparable to the screening length as shown in Table I, the impurity density in our discrete impurity model could be safely used to extract the value of mobility from the traditional mobility model. We should point out, however, that this accidental similarity between the screening length and mean-separation of impurities is true only for bulk Si. In the cases of III-V compound semiconductors or low-dimensional structures, this similarity breaks down and, strictly speaking, the usage of "mobility" in DD simulations becomes more questionable in such cases.

We would like to stress that this argument makes sense only if the impurity potential is separated into the long- and short-range parts so that only the short-range part of the potential is treated as scattering potential and excluded from the Poisson equation. Otherwise, the long-range part of the impurity potential would overlap among impurities and the scattering potential of each impurity could not be regarded as identical and, thus, the last equality of Eq. (4) breaks down. In other words, the exact location of impurities matters only for the long-range part of the impurity potential in the Poisson equation and is irrelevant for the short-range scattering potential in the current-continuity equation.

D. Fluctuation-Dissipation Theorem under Discrete Impurities

In the present discrete impurity model, the "long-range" potential modulation shows up explicitly in the subthreshold regimes with a small drain voltage and the carrier density is *locally* modulated around impurities. Therefore, under quasi-equilibrium, the "local" diffusion current induced by such density modulation needs to be balanced by the "local" drift current induced by potential modulation around impurities. This is one of the physical contexts of the fluctuation-dissipation theorem [20]. The electrostatic potential under the discrete impurities is then separated into two terms;

$$\phi\left(\mathbf{r}\right) = \bar{\phi} + \delta\phi\left(\mathbf{r}\right), \tag{5}$$

where $\bar{\phi}$ is the electrostatic potential caused by the jellium impurity and $\delta\phi\left(\mathbf{r}\right)$ is the "long-range" potential modulation associated with discrete impurities. Notice that $\bar{\phi}$ is identical to the potential induced by the zero Fourier component of the microscopic impurity density $N_{imp}^{micro}\left(\mathbf{r}\right)$. Strictly speaking, $\bar{\phi}$ is also dependent of position through the spatial variation of the jellium impurity density $\bar{N}_{imp}$. Its variation is, however, very gradual compared with that of $\delta\phi\left(\mathbf{r}\right)$ and could be ignored in the present arguments. According to statistical mechanics, the (classical) electron density under quasi-equilibrium of the linear response regimes is modulated in accordance with Eq. (5), namely,

$$n\left(\mathbf{r}\right) = n_{\phi=0} e^{\frac{e\phi\left(\mathbf{r}\right)}{k_B T}} \approx \bar{n}\left[1 + \frac{e}{k_B T}\delta\phi\left(\mathbf{r}\right)\right] \equiv \bar{n} + \delta n\left(\mathbf{r}\right), \tag{6}$$

where $\bar{n} = n_{\phi=0}\exp\left(e\bar{\phi}/k_B T\right)$, k_B is the Boltzmann constant, T is temperature, and $\delta n\left(\mathbf{r}\right)$ is the density modulation associated with $\delta\phi\left(\mathbf{r}\right)$; $\delta n = e\bar{n}\delta\phi/k_B T$. Here, we have used the linear approximation such that the density modulation is proportional to the potential modulation. This is consistent with the Thomas-Fermi approximation employed in constructing the discrete impurity model.

The diffusion current density induced by the local density modulation $\delta n\left(\mathbf{r}\right)$ is then given by

$$\mathbf{J}_{n,D}^{local}\left(\mathbf{r}\right) \approx eD_n\bar{n}\frac{e}{k_B T}\frac{\partial\delta\phi\left(\mathbf{r}\right)}{\partial\mathbf{r}}. \tag{7}$$

Notice that this is justified because $\delta\phi$ represents the "long-range" potential modulation, which is longer than a screening length, and hence, a mean-free-path. Under quasi-equilibrium, Einstein's relation (the fluctuation-dissipation theorem), $D_n = \left(k_B T/e\right)\mu_n$, must hold. Hence, $\mathbf{J}_{n,D}^{local}\left(\mathbf{r}\right)$ induced by $\delta n\left(\mathbf{r}\right)$ becomes identical (except its sign) to the local drift current density $\mathbf{J}_{n,\mu}^{local}\left(\mathbf{r}\right)$ induced by $\delta\phi\left(\mathbf{r}\right)$;

$$\mathbf{J}_{n,D}^{local}\left(\mathbf{r}\right) = -e\bar{n}\mu_n\left(-\frac{\partial\delta\phi\left(\mathbf{r}\right)}{\partial\mathbf{r}}\right) = -\mathbf{J}_{n,\mu}^{local}\left(\mathbf{r}\right). \tag{8}$$

Therefore, the local diffusion current is exactly balanced with the local drift current under quasi-equilibrium, even when impurities are represented as discrete in the Poisson equation. Furthermore, Eq. (8) clearly indicates that the value of μ_n should be interpreted as the one under the average electron

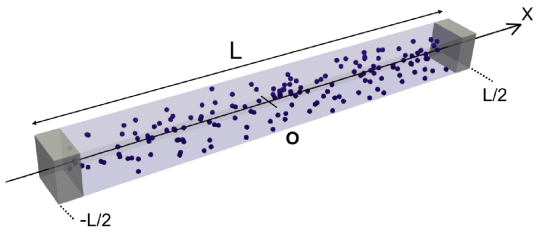

Fig. 1. Schematic drawing of the resistor structure employed in DD simulations. The discrete donor impurities are randomly distributed in the substrate and represented by solid dots. The colored (grey) regions near the contacts represent the jellium impurity regions.

density $\bar{n}$ or, equivalently, $\bar{N}_{imp}$. This justifies the use of the impurity density spread in space to extract the value of μ_n from the impurity-density dependent mobility model in the current-continuity equation.

This argument breaks down when the "short-range" part of the impurity potential is also included in $\delta\phi(\mathbf{r})$ in Eq. (5) by localizing the impurity charge at each impurity site. In that case, $\delta n(\mathbf{r})$ in Eq. (6) becomes unrealistically large at impurity sites. This implies that electrons are trapped by impurities and cannot represent free carriers. As a result, the balance between the diffusion and drift currents associated with local modulations in density and potential is broken. In other words, the concept of mobility and, hence, Einstein's relation break down at the length-scale shorter than a mean-free-path. This leads to an artificial threshold voltage shift in MOSFETs, as observed in early 'atomistic' DD simulations with point charge impurities [3]–[5], because the impurity density in the semiconductor substrate is effectively lowered due to the carriers trapped by deep impurity potentials [7].

III. Simulation Results and Discussion

A. Device Structure and Impurity Localized Models

We employ a simple resistor structure for DD simulations, as shown in Fig. 1, in which the discrete donor impurities are randomly distributed in silicon substrate and represented by solid dots. The grey regions at the endpoints with the length of 20 or 10 nm represent the jellium impurity regions where the continuous impurity density is assumed. Inserting the jellium regions in the substrate is required in the cases of localized impurity models (as will be defined below) to avoid potential discontinuity taking place at the contacts where the fixed boundary condition is applied [3], [4]. Although this kind of problem does not arise in our discrete impurity model, the same device structure including the jellium regions is used for all impurity models to make fair comparisons. The average impurity density is assumed to be $\bar{N}_{imp} = 10^{18}$, 10^{19} or 10^{20} cm^{-3}. The length of the resistor is $L = 440$ nm with the mesh spacing of $a = 1$ nm for $\bar{N}_{imp} = 10^{18}$ cm^{-3} and $L = 120$ nm with $a = 0.5$ nm for $\bar{N}_{imp} = 10^{19}$, 10^{20} cm^{-3}. The cross-sectional area is $S = 20 \times 20$ nm^2. The length and cross-sectional area are intentionally made large so that the effects associated with the interface (boundary) and quantum confinement are insignificant.

In order to represent the discrete nature of impurities in DD simulations, we employ, in addition to the present discrete impurity model given by Eq. (3) (referred to the long-range model in the present section), the following three localized impurity models,

(1) Exponential localized model;

$$\rho_Y^{local}(\mathbf{r}) = \frac{e}{4\pi a^2}\frac{e^{-r/a}}{r}, \tag{9}$$

(2) Gaussian localized model;

$$\rho_G^{local}(\mathbf{r}) = \frac{e}{(2\pi a^2)^{3/2}} e^{-\frac{r^2}{2a^2}}, \tag{10}$$

(3) NGP (Nearest-Grid-Point) localized model;

$$\rho_{NGP}^{local}(\mathbf{r}) = \frac{e}{a^3}\theta\left(\frac{a}{2}-|x|\right)\theta\left(\frac{a}{2}-|y|\right)\theta\left(\frac{a}{2}-|z|\right). \tag{11}$$

Here, a is the mesh-spacing employed in DD simulations. Hence, an impurity charge in the above formulas is localized in the region comparable to a and the localization is strongest in the NGP localized model. Notice that Eqs. (3) and (9) have the same functional form. However, q_c is fixed at the screening length in Eq. (3), whereas a in Eq. (9) is, of course, dependent of the mesh used in DD simulations.

B. Drift-Diffusion Simulation Results

Fig. 2 shows the electrostatic potential, electron mobility, and electron density along the x-axis obtained from the DD simulations under a specific impurity configuration in the resistor ($L = 120$ nm) with $\bar{N}_{imp} = 10^{19}$ cm^{-3}. The four different impurity models, namely, the long-range model and three localized models defined above, are employed. The electron mobility is locally evaluated from the impurity-density dependent mobility model and, thus, simply reflects the local impurity density in each discrete impurity model. The horizontal dotted lines represent the values obtained from the DD simulations under the jellium impurity. The shaded regions at both endpoints are the jellium impurity regions.

The electrostatic potential is, of course, more spiky as the impurity density is more localized in space. However, the magnitude of the potential fluctuations induced by the long-range model is much smaller than that estimated from the long-range part of the bare impurity potential: The potential fluctuations due to the long-range part of the bare impurity potential are listed in Table I. This observation clearly demonstrates that the long-range part of the impurity potential is mostly screened by carriers and that the short-range part of the impurity potential is properly excluded from the Poisson equation in the long-range model. The electron mobilities in the localized models are much larger than that in the long-range model. In particular, the electron mobility in the NGP localized model is given by the phonon-limited mobility (~ 1400 cm^2/V·s) in most regions and the average mobility tends to be much larger than that in the jellium impurity. Furthermore, the overall electron density in the NGP localized model is greatly reduced in the discrete impurity region, compared with that in the (shaded) jellium regions. This is because electrons are trapped at impurity sites by deep impurity potential and the substrate impurity density is effectively lowered.

We have carried out about one hundred DD simulations by varying the impurity configurations in the resistors and

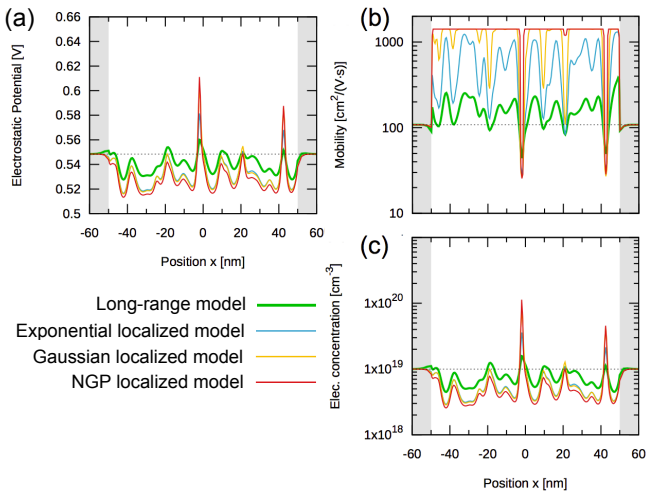

Fig. 2. (a) Electrostatic potential, (b) electron mobility, and (c) electron density along the x-axis obtained from the DD simulations with four different impurity models (the long-range model and three localized models) for the resistor ($L = 120$ nm) with $\bar{N}_{imp} = 10^{19}$ cm^{-3}. The horizontal dotted lines represent the values obtained from the DD simulations under the jellium impurity and the shaded regions at both endpoints are the jellium impurity regions.

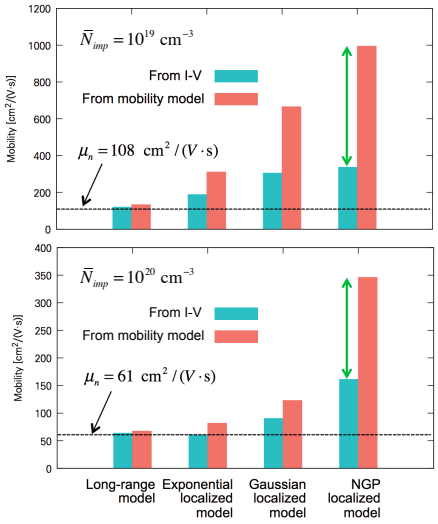

Fig. 3. Average electron mobilities of the resistor of $L = 120$ nm with (Top) $\bar{N}_{imp} = 10^{19}$ and (Bottom) 10^{20} cm^{-3} obtained from one hundred DD simulations by varying the impurity configurations. The average mobility is calculated by two different methods as explained in the text and denoted by "From I-V" and "From mobility model." The horizontal dotted lines represent the values obtained from the DD simulations under the jellium impurity.

confirmed that the above results are quite universal no matter how impurities are configured. The average mobility is calculated by two different methods: The current-voltage (I-V) characteristics from DD simulations are used to find the resistance R and mobilities are calculated from the formula, $\mu_n = L/(e\bar{n}SR)$. Then, they are averaged over all impurity configurations. The calculation results are shown in Fig. 3 (denoted by "From I-V") for $\bar{N}_{imp} = 10^{19}$ and 10^{20} cm^{-3}. In the other method, the local mobilities extracted from the impurity-density dependent mobility model (as done in Fig. 2) are averaged over both position and impurity configurations (denoted by "From mobility model"). The horizontal dotted lines in Fig. 3 represent the values under the jellium impurity. It is clear that the average mobilities obtained from the two methods are very close to each other in the long-range model and similar to the value under the jellium impurity. On the other hand, the localized models overestimate the average mobility, and the mobilities obtained from the two methods are quite different. Since the localized models strongly depend on the mesh-size employed in DD simulations, the present results for the localized impurity models are even optimistic because of relatively large mesh-size employed ($a = 0.5$ nm). Nevertheless, the NGP localized model yields the largest mobility among the localized models and the discrepancy of the average mobilities obtained from the two different methods is very large, as indicated by arrows in Fig. 3.

This discrepancy in average mobility for the NGP localized model is explained as follows. Fig. 4 shows the internal potential and polarization charge density along the resistor for $\bar{N}_{imp} = 10^{19}$ and 10^{20} cm^{-3}. Here, the internal potential at position x is defined by $\phi^{av}_{int}(x) = \phi^{av}_{V}(x) - \phi^{av}_{V=0}(x) - \Delta V(x)$, where $\phi^{av}_{V}(x)$ is the potential averaged over impurity configurations when the voltage V is applied and $\phi^{av}_{V=0}(x)$ is the one when no voltage is applied. $\Delta V(x)$ $(= xV/L)$

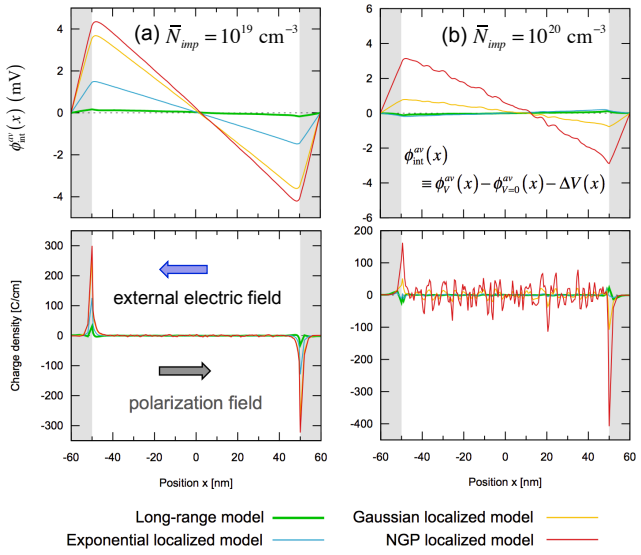

Fig. 4. (Top) Internal potential and (Bottom) polarization charge density along the resistor of $L = 120$ nm for (a) $\bar{N}_{imp} = 10^{19}$ and (b) 10^{20} cm^{-3}.

is the potential increment at x due to V. Therefore, $\phi^{av}_{int}(x)$ represents the potential obtained by eliminating all external and fluctuating potentials associated with discrete impurities and, thus, should be zero over the resistor in the ideal case. We find that $\phi^{av}_{int}(x)$ is nearly zero in the long-range model, whereas very strong polarization charges, obtained from the second derivative of $\phi^{av}_{int}(x)$, arise at the boundaries between discrete and jellium impurity regions in the NGP localized model. This is due to the discontinuity of mobility at the boundaries: In the discrete impurity region, electron mobility in the NGP localized model is nearly phonon-limited, whereas in the (shaded) jellium regions it suddenly drops

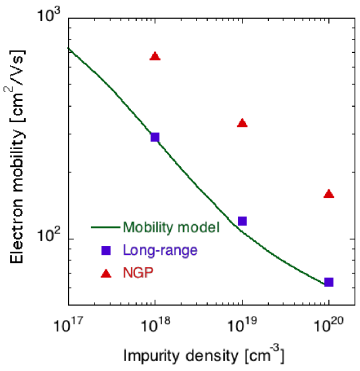

Fig. 5. Electron mobility in Si obtained from the DD simulations with the long-range model and the NGP localized model as a function of impurity density. The solid line represents the curve of the impurity-density dependent mobility model fitted to the experimental mobilities.

to the impurity-limited mobility, as shown in Fig. 2. As a result, electrons are accumulated or depleted at the boundaries between the two regions and a strong polarization field arises against the external electric field. The current in the NGP localized models is then reduced compared with that under the jellium impurity, and so is the average mobility.

The polarization field found in Fig. 4 is, of course, an artifact and this finding supports our claims that the usage of the localized impurity models to extract the value of mobility from the traditional mobility model is inconsistent with the framework of the DD simulation. On the other hand, the long-range impurity model leads to similar mobilities to those from the jellium impurity. This is confirmed from Fig. 5, in which electron mobilities obtained from the DD simulations with the long-range model and the NGP localized model are plotted as a function of impurity density. The mobilities evaluated from the I-V characteristics are used. The solid line shows the mobility of the impurity-density dependent mobility model fitted to the experimental results. The long-range model indeed reproduces the correct mobility at any impurity densities, whereas the NGP localized model largely overestimates the mobility.

IV. Conclusion

We have discussed the fundamental aspects of physical modeling associated with discrete impurities under the framework of the DD simulation scheme. The physical interpretations of the potential fluctuations, mobility, and an appropriate discrete impurity model to represent the discrete nature of impurities in DD simulations have been theoretically discussed. The present analysis has been validated in DD simulations by showing that the traditional mobility model could be safely used in our discrete impurity model, whereas the localized impurity model induces an unphysical polarization field in the substrate and is unable to reproduce the correct mobility.

Acknowledgment

The authors would like to thank K. Matsuzawa and Y. Akiyama of KIOXIA Corporation (former Toshiba Memory Corporation) for fruitful discussion.

References

[1] N. Zographos, C. Zechner, I. Martin-Bragado, K. Lee, and Y.-S. Oh, "Multiscale modeling of doping processes in advanced semiconductor devices," *Materials Science in Semiconductor Processing*, vol. 62, pp. 49–61, May 2017, doi: 10.1016/j.mssp.2016.10.037.

[2] M. Miranda, "When every atom counts," *IEEE Spectrum*, vol. 49, no. 7, pp. 32–32, July 2012, doi: 10.1109/MSPEC.2012.6221080.

[3] H.-P. Wong and Y. Taur, "Three-dimensional "atomistic" simulation of discrete random dopant distribution effects in sub-0.1 μm mosfet's," in *Proceedings of IEEE International Electron Devices Meeting*, Dec. 1993, pp. 705–708, doi: 10.1109/IEDM.1993.347215.

[4] A. Asenov, "Random dopant induced threshold voltage lowering and fluctuations in sub-0.1 μm mosfet's: A 3-d "atomistic" simulation study," *IEEE Transactions on Electron Devices*, vol. 45, no. 12, pp. 2505–2513, Dec. 1998, doi: 10.1109/16.735728.

[5] D. J. Frank, Y. Taur, M. Ieong, and H.-P. Wong, "Monte carlo modeling of threshold variation due to dopant fluctuations," in *1999 Symposium on VLSI Circuits. Digest of Papers*, June 1999, pp. 171–172, doi: 10.1109/VLSIT.1999.799397.

[6] N. Sano, K. Matsuzawa, M. Mukai, and N. Nakayama, "Role of long-range and short-range coulomb potentials in threshold characteristics under discrete dopants in sub-0.1 μm si-mosfets," in *Technical Digest. Int. Electron Device Meeting*, Dec Dec. 2000, pp. 275–278, doi: 10.1109/IEDM.2000.904310.

[7] N. Sano, K. Matsuzawa, M. Mukai, and N. Nakayama, "On discrete random dopant modeling in drift-diffusion simulations: physical meaning of 'atomistic' dopants," *Microelectronics Reliability*, vol. 42, no. 2, pp. 189–199, Feb. 2002, doi: 10.1016/S0026-2714(01)00138-X.

[8] N. Damrongplasit, S. H. Kim, and T. K. Liu, "Study of random dopant fluctuation induced variability in the raised-ge-source tfet," *IEEE Electron Device Letters*, vol. 34, no. 2, pp. 184–186, Feb. 2013, doi: 10.1109/LED.2012.2235404.

[9] J. Yoon and R. Baek, "Study on random dopant fluctuation in core shell tunneling field-effect transistors," *IEEE Transactions on Electron Devices*, vol. 65, no. 8, pp. 3131–3135, Aug. 2018, doi: 10.1109/TED.2018.2846782.

[10] K. Liu and E. Chen, "Investigation of the effects and the random-dopant-induced variations of source/drain extension of 7-nm strained sige n-type finfets," *IEEE Transactions on Electron Devices*, vol. 66, no. 2, pp. 847–854, Feb. 2019, doi: 10.1109/TED.2018.2884246.

[11] N. Sano, "Physical issues in device modeling: Length-scale, disorder, and phase interference," in *2017 International Conference on Simulation of Semiconductor Processes and Devices*, Sept. 2017, pp. 1–4, doi: 10.23919/SISPAD.2017.8085249.

[12] N. Sano, K. Yoshida, C.-W. Yao, and H. Watanabe, "Physics of discrete impurities under the framework of device simulations for nanostructure devices," *Materials*, vol. 11, no. 12, p. 2559, Dec. 2018, doi: 10.3390/ma11122559.

[13] H. Yu, D. Kim, S. Rhee, S. Choi, and Y. J. Park, "A mobility model for random discrete dopants and application to the current drivability of dram cell," *IEEE Transactions on Electron Devices*, vol. 64, no. 10, pp. 4246–4251, Oct. 2017, doi: 10.1109/TED.2017.2741968.

[14] K. Huang, *Statistical Mechanics*, 2nd ed. New York, U.S.A.: John Wiely & Sons, 1987.

[15] M. V. Fischetti and W. G. Vandenberghe, *Advanced Physics of Electron Transport in Semiconductors and Nanostructures*, New York, U.S.A.: Springer, 2016.

[16] K. Yoshida, K. Tsukahara, and N. Sano, "Polarization effect due to discreteness of dopants in nanoscale mosfets," *IEEE Transactions on Electron Devices*, vol. 66, no. 10, pp. 4343–4347, Oct. 2019, doi: 10.1109/TED.2019.2935503.

[17] T. Fukui, T. Uechi, and N. Sano, "Three-dimensional Monte Carlo simulation of electron transport in Si including full coulomb interaction," *Applied Physics Express*, vol. 1, p. 051407, May 2008, doi: 10.1143/APEX.1.051407.

[18] K. Nakanishi, T. Uechi, and N. Sano, "Self-consistent Monte Carlo device simulations under nano-scale device structures: Role of Coulomb interaction, degeneracy, and boundary condition," in *Technical Digest. Int. Electron Device Meeting*, pp. 1–4, Dec. 2009, doi: 10.1109/IEDM.2009.5424417.

[19] C. Jacoboni, *Theory of Electron Transport in Semiconductors: A Pathway from Elementary Physics to Nonequilibrium Green Functions*. New York, U.S.A.: Springer, 2010.

[20] R. Kubo, M. Toda, and N. Hashitsume, *Statistical Physics II: Nonequilibrium Statistical Mechanics*, 2nd ed. Berlin, Germany: Springer, 1991.